Electric Fano resonance-based terahertz metasensors

Ride Wang Lei Xu Jiayi Wang Lang Sun Yanan Jiao Yuan Meng Shuo Chen Chao Chang Chunhai Fan**

Ride Wang, Lang Sun, Shuo Chen, Chao Chang
Innovation Laboratory of Terahertz Biophysics, National Innovation Institute of Defense Technology, Beijing, 100071, China
Email Address:changc@xjtu.edu.cn
Chao Chang
Xi'an Jiaotong University, Shaanxi, 710049, China
Lei Xu
Advanced Optics and Photonics Laboratory, Department of Engineering, School of Science and Technology, Nottingham Trent University, Nottingham NG11 8NS, UK
Jiayi Wang
Key Laboratory of Weak-Light Nonlinear Photonics, Ministry of Education, TEDA Institute of Applied Physics and School of Physics, Nankai University, Tianjin 300457, China
Yanan Jiao
Department of General Surgery, First Medical Center of Chinese PLA General Hospital, Beijing 100853, People's Republic of China.
Yuan Meng
Key Laboratory of Photonics Control Technology of the Ministry of Education, Tsinghua University.
Chunhai Fan
School of Chemistry and Chemical Engineering Shanghai Jiao Tong University Shanghai 200240, China
Email Address:fchh@sinap.ac.cn

Keywords: *quasi-BIC Fano resonance, metasensors, terahertz*

Sensing technologies based on terahertz (THz) waves have significant application prospects in fast imaging, free label, and non-invasive inspection methods. However, the main drawback limiting the performance of terahertz-based bio-chemical sensors is the weak interaction between the optical field and the analyte, leading to low sensitivity. Herein, we present an ultra-sensitive THz metasensor based on electric Fano resonant metasurface which consists of three gold microrods arranged periodically. The designed electric Fano resonance provides a strong near-field enhancement near the surface of our microstructure, significantly boosting light-analyte interactions and thus the sensitivity. Such an electric Fano resonance is formed by the interference between a leaky electric dipole resonance and a bounded toroidal dipole mode which is a symmetry-protected bound state in the continuum supported by the sub-diffractive periodic system here. A perturbation was introduced as a leakage channel in the form of a quasi-BIC to observe the infinite-Q-factor ideal BIC in the experiment, which was in accordance with the analogue one. Furthermore, the proposed structure could help distinguish extremely dilute concentrations (nM) of solutions, indicating its strong biosensing ability that relies on resonator enhancement in the near-field intensifying the interaction between light and matter. Our results are expected to help realize a non-destructive and non-contact quantitative inspection of low-concentration solutions, providing a useful sensing approach for disease prevention and diagnosis.

1 Introduction

Metasurfaces for arbitrary control and manipulation of the amplitude, phase, and polarization state of light with a subwavelength spatial resolution can be applied to a wide range of desired optical functionalities,[1, 2] including computational imaging,[3] lasing spaser,[4] polychromatic holography,[5, 6, 7] and achromatic metalenses.[8] The excellent model of a metasurface is composed of subwavelength microrods (or slots) with in-plane variable geometric parameters, such as the orientation, dimension, and shape, forming an inhomogeneous and anisotropic optical field distribution, which can be engineered to control the optical responses in a desired manner.[9, 10, 11, 12, 13] The focus of research so far has been on combining or tailoring the microrods to manipulate light more efficiently based on optically induced electric and magnetic Mie-type resonances to explore cutting-edge applications and innovative physics, such as enhanced nonlinear generation,[14, 15] optical sensing,[16] and molecular barcoding.[17] The resonant response of metasurfaces because of their high quality (Q) factor allows to strongly enhance the local op-

tical near-fields and promote light-matter interactions at a specific frequency within subwavelength resonators.

Realized high-Q response are earlier mainly associated with Fano resonances at the geometric tailoring of the subwavelength structures platform introduced the asymmetry in a unit cell.[18, 19, 20] The featured sharp asymmetric spectral line profiles arise from the close interaction between a discrete (subradiant) mode and a continuum (superradiant) mode.[21, 22] This process, at the Fano resonance, is accompanied by a weak scattering light coupled into free space, resulting in a drastic suppression of the radiation loss in metasurface systems. Numerous designs have been proposed by modifying the geometry of the sub-unit or by introducing asymmetric parameters into ring/disk cavities,[23] holes,[24] dolmen structures,[25] and compound sub-structures.[26] Furthermore, to improve the ability of confining light at resonance and to reduce the leakage rate, generating ultrahigh-Q resonances have been linked to the bound state in continuum (BIC),[27, 28, 29] which is an area of growing interest. An ideal BIC exhibits infinite lifetime and vanishing resonance width, which can exist only in lossless infinite structures with a perfectly confined nonradiative mode. In a real system, ideal BIC is not a directly detectible state, which can be investigated only through quasi-BIC in the form of a supercavity mode with the loss of induced perturbations. Indeed, quasi-BICs provide an elegant approach to control light-matter interaction given their ultrahigh-Q associated with a significant enhancement in the near-field. In detail, the quasi-BIC mode has been elaborated in metasurfaces formed by symmetric dielectric dimer nanobar structures[30] or asymmetric metal dipole bars[31] in the unit cell for normal incidence, which have been used for many serviceable functionalities such as nano-film sensing,[32, 33] nonlinear generation enhancement,[30] and lasing.[4] Among, research on quasi-BIC corresponding to toroidal dipoles (TDs) has been particularly concerned.[34, 35] TDs possess promising applications in the formation of non-radiating anapole states and in enhancing the energy localization by concentrating time.[36] Furthermore, TD BIC usually associated with the excitation of electric dipole (ED) moment, the total near-field enhancement can be obtained for both inside the unit and near the surface of the structure, providing multiple opportunities for enhance light-matter interactions. Meanwhile, designing metasurfaces with a TD response present electromagnetic scenarios such as observation of a higher-order topological,[37, 38] resonant transparency,[39] and bridging Huygens' metasurfaces.[29] These excellent properties can further extend the unprecedented functions and improve the performance of devices.

Terahertz (THz) technology provides a highly effective means for security screening, nonionizing, nondestructive sensing applications since THz waves have excellent characteristics, such as low photon energy and strong penetrability.[40, 41, 42, 43] However, owing to the lack of powerful radiation sources and the mismatch between the THz wavelength and the scattering cross-section of the analyte, the inter- or intra-molecular vibration of the analyte in the THz region is quite weak, which significantly limits the development of THz technology in sensing applications. Combined with ultrahigh-Q metasurfaces, the encountered challenges in sensing research would be addressed.

In this work, a quasi-BIC Fano resonance was comprehensively demonstrated in a THz metasurface composed of composite microrods based on the coupling of leaky ED resonance and bounded TD modes. The TD resonance results from the head-to-tail arrangement of the magnetic dipole-type excitation, which is further confirmed by the spherical multipolar expansion of the induced current density. The features of the BIC are experimentally observed by adjusting the dimension of the mid-microrod, which transforms ideal BIC into a leaky resonance with a large Q-factor. The results are in good agreement with full-wave numerical calculations. Owing to the strong electromagnetic near-field enhancement of the resonator, in addition, the simple model for the arrays of a detuned-resonant-dipole trimer is excavated to render a high biosensing capability by boosting light-matter interaction, which can help clearly discriminate low-concentration (nM) solutions. With the versatility and strong evanescent field provided by metal metasurfaces, the designed resonator as a powerful and convenient tool is expected to be employed in the high-performance sensing of trace biological and chemical substances.

The electromagnetic response of an infinite 2D metasurface comprising identical resonator units with three gold building blocks was analyzed. Figure 1a shows the perspective view of the proposed THz metasensor. The typical partial portion of the metasurface was fabricated on a 1 mm thick quartz substrate,

and the inset reveals enlarged geometrical dimensions of the unit cell in Figure 1b. The sample was patterned using convention photolithography, followed by magnetron sputtering of a 100 nm gold metal and a lift-off process, leaving behind the resonator array. The individual resonator has a square period with a pitch of $p \times p = 100\ \mu\text{m} \times 100\ \mu\text{m}$ in both x and y directions. The width of the microrods is $w = 10\ \mu\text{m}$. The length of the microrods on both sides of the resonator is fixed at $L_1 = 70\ \mu\text{m}$, while the dimension of the mid-microrod can be varied to study the special electromagnetic properties of the structure. Microrods are separated by a distance $d = 32\ \mu\text{m}$ along the x-axis whose long axis is aligned with the y-axis. To validate the response of the designed metasurface, numerical calculations based on 3D finite-difference time-domain (FDTD) solution software are employed. Periodic boundary conditions were employed along the x- and y-directions to illustrate the periodic structure, and the perfectly matched layer (PML) absorbing boundary condition was applied in the z-direction in the free space. Convergent results could be obtained by setting the mesh sizes smaller than the corresponding minimum dimension of construction. The material of the microrods was set to perfect electrical conductor (PEC) on account of the conductivity of the conventional metal in the THz region at the order of $10^7\ \text{S}\cdot\text{m}^{-1}$ so that the Ohmic loss is largely suppressed. The excitation of the resonances with normal-incidence y-polarized THz electric field leads to a distinct asymmetric Fano lineshape ($f = 1.17$ THz) with a characteristic dip/peak pair profile and a higher frequency resonance ($f = 1.42$ THz) with detuned $L_2 = 55\ \mu\text{m}$, as shown in Figure 1c. The inset shows the E_z electric field distribution of the lower resonance frequency, which displays the electric vibration of the microrods corresponding to the coupling mode. We observed significant near-field enhancement of the electric field (35-fold) in the resonator in the Figure S1 of the Supplemental Material. The higher-frequency resonance results from the coupling of the Fano resonance to the first-order lattice mode of the metasurface array with stronger field confinement.[44]

Here, we focus on the lower Fano resonance. Combined with the spherical multipolar decomposition theory, we decompose the surface current of the resonator to explain the coupling components of the modes. As shown in Figure 2a,b, the optical response is dominated by strong ED and TD excitations. By control the length the microrod in the center, the coupling between the ED mode p_y and the nonradiating TD mode can be flexibly tuned, thus the Q-factor of the electric Fano-resonance shape can be adjusted on demand. Figure 2c gives the electric near-field distributions in XY plane. As can be seen, a pronounced poloidal current distribution is clearly formed from the three microrods. Furthermore, the closed electric current for neighboring microrods brings about a head-to-tail circulating magnetic field arrangement at the XZ plane which results in a TD ($\overrightarrow{T}$) resonance excitation as shown in Figure 2d, indicating the excitation of TD BIC here. Based on the right-hand principle, the toroidal moment points in the y-direction and is coupled with the bright electric dipole momentum, leading to a sharp Fano resonance quasi-BIC.

An analysis of the effect of altering the dimension of the mid-microrod on the transmission of ideal-to-quasi BIC was carried out. In the experiment, the characteristic configurations were measured using a fiber-based 4-f far-field THz time-domain spectroscopy system at normal incidence. A THz beam with a 2 mm diameter spot illuminated the metasurface sample with a size of $5 \times 5\ \text{mm}^2$. The THz electrical signals of the transmission pulse varying with time were measured $E_m(t)$ and $E_{ref}(t)$ (quartz substrate) with and without the metasurface in dry nitrogen atmosphere. Subsequently, by applying a fast Fourier transform, we obtained normalized transmittance $T = |E_m(f)| \,/\, |E_{ref}(f)|$. The BICs could only be observed by introducing a leakage channel into the unit cell from ideal bound states due to the distortion of the symmetry protection. The transitions from BICs to sharp quasi-BIC feature response are visualized in both simulations and experiments in Figure 3a-c. The two trajectories presented are the evolutions of the transmission dips in the simulation and experimental spectra with different L_2, the trends of which are consistent with that shown in Figure 3a,c. The spectral linewidth gradually narrows as L_2 approaches mixed L_1, which reflects a decreasing leakage rate of quasi-BIC. The resonance frequency displays evident red-shift as L_2 increases. Until the perturbation is reduced toward zero, i.e., $L_2 = 70\ \mu\text{m}$, the resonance linewidth vanishes, and the transmission valley disappears, in which the symmetry-protected BIC state with infinite Q-factor increases. With the excitation of the quasi-BIC mode, one can engineer the Q-factor of the resonance and control the radiation damping rate. Notably, despite the fact

that a slight perturbation can result in an infinitely low leakage of the BIC in theory, it remains challenging to measure resonant linewidths narrower than 3.8 GHz (130 s time integral) because of the resolution limitation of our equipment. We fit the transmission intensity spectrum with a typical Fano lineshape formula

$$T_{Fano} = |a_1 + ja_2 + \frac{b}{\omega - \omega_0 + j\gamma}|^2$$

to extract the leakage rate, where the a_1, a_2, and b are real constant factors, ω_0 and γ are the resonance frequency and the damping rate, respectively. By inducing the asymmetry parameter $a = L_2 - L_1$, we map the divergence trajectory of the Q factor with different a, as illustrated in Figure 3d, retrieved from the Fano shape in Figure 3b,c. The Q-factor of quasi-BIC evidently tends to infinity at $a = 0$ μm, which indicates that no amount of energy radiates into free space due to the symmetry-protected BIC. The discussion on advantages of trimer is that one can find the similar electric and magnetic field distribution between BIC and quasi-BIC in Figure S2 of the Supplement Material, which indicate the quasi-BIC resonance inherited the BIC characteristics. However, the experimental values of the Q factors are generally lower than the simulated values as both radiative and nonradiative losses affect the measured linewidth of the resonances. The inevitable scattering losses due to the rough surfaces and finite area of the samples also account for the decrease in the Q factor. Although the measured Q-factor values were not good enough to reach the expectation, the reported BIC model theoretically predicts an infinite radiative quality factor in an ideal scenario. Meanwhile, we experimentally confirmed BIC features of a subwavelength metasurface and observed optical quasi-bound states in a symmetry-compatible radiation continuum.

Furthermore, we analyzed the sensitivity of the proposed metasensor by varying the refractive index and maintaining a constant thickness of the analyte. The relationship between the resonance drifts and the refractive index of the analyte was established to verify the device performance. Figure 4a shows the shift results in case of $L_2 = 55$ μm with a 6 μm thick analyte but different refractive indices at quasi-BIC resonance. An evident shift in the resonance frequency is observed at approximately 93 GHz when varying the refractive index from $n = 1$ to $n = 1.5$. The sensitivity of the metasensor was defined as $S = \Delta f/\Delta n$, where Δf is the frequency shift due to the coating of the analyte on the metasurface, and Δn is the per unit change in the analyte refractive index. The quasi-BIC Fano resonance sensitivity was found to be 165 GHz/refractive index unit (RIU), as shown in Figure 4b.

To explicitly present the high sensitivity of the proposed sensing technology, we carried out detailed experiments on quasi-BIC Fano resonance with different trace liquid concentrations. As an example, we targeted Interleukin-6 (IL-6), which is a multifunctional cytokine with a wide range of biological activities. It plays an important role in immune response, inflammatory response, hematopoietic regulation, and tumor immunity. The detection of IL-6 concentration is of great significance for the diagnosis of many clinical diseases.[45, 46] We configured uniform the aqueous phosphate buffer solution (PBS, 0.05 M K_2HPO_4 and 0.05 M KH_2PO_4, pH 7.0, named as No IL-6) and the aqueous PBS with different concentrations of IL-6 (named as 1, 10, 50, and 100 nM IL-6) in it. We take a sufficient amount of the solution and drop it on the metasurface. With a directly squashing technique using quartz cover, the sample is prepared for measurement when the moisture was completely volatilized, as shown in the Figure 5a. The THz transmission properties were affected by the dielectric properties of liquid media with different concentration. The top panel of Figure 5b experimentally compares the measured transmission properties of the without PBS (black solid lines) and with PBS (No IL-6). On increasing IL-6 concentration, the response of the resonator is significantly red-shifted. Notably, the design can clearly identify the solution with a solubility difference of 1 nM. Compared with the top panel, the resonant frequency shift for a concentration of 1 nM is 23 GHz more than that for a concentration of 0 nM. These examples demonstrated that the possibility of using this technology to serve as real-time sensors to develop convenient and portable THz devices for inspecting biological and chemical trace substances changes.

2 Conclusion

In summary, we experimentally demonstrated an ultrasensitive THz metasensor based on quasi-BIC Fano resonance, which can sense solutions with ∼nM concentrations. A comprehensive analysis of the resonator comprising composite microrods, which lead to a sharp resonance with significant enhancement in the high-Q factor, was provided. The Fano resonance can be attributed to the coupling between the leaky ED and bounded TD modes. The physical mechanism of the excited mode coupling was analyzed by decomposing the surface current of the resonator via the spherical multipolar theory and imaging the electrical and magnetic near-field distributions. Meanwhile, by introducing a perturbation into the resonator, the transmission spectra were varied from infinite Q-factor symmetry-protected BIC to observable quasi-BIC. The electric field of metallic metasurface are mainly localized around the matal/dielectic interface. In contrast, for dielectric metasurface, nearly all energy is concentrated in the dielectric, which is extremely adverse to sensing application. This work explored the promising possibilities of THz metasurfaces in ultrasensitive sensing, which provides a reference scheme for the real-time on-chip detection of trace or low-concentration chemicals and biomolecules.

Acknowledgements
C.C. acknowledges the support from the XPLORER PRIZE.

Conflict of interest
The authors declare no conflict of interest.

References

[1] N. Yu, F. Capasso, *Nature Materials* **2014**, *13*, 2 139.

[2] S. Sun, Q. He, J. Hao, S. Xiao, L. Zhou, *Advances in Optics and Photonics* **2019**, *11*, 2 380.

[3] S. Colburn, A. Zhan, A. Majumdar, *Science Advances* **2018**, *4*, 2 eaar2114.

[4] A. Kodigala, T. Lepetit, Q. Gu, B. Bahari, Y. Fainman, B. Kante, *Nature* **2017**, *541*, 7636 196.

[5] W. T. Chen, K. Y. Yang, C. M. Wang, Y. W. Huang, G. Sun, I. D. Chiang, C. Y. Liao, W. L. Hsu, H. T. Lin, S. Sun, L. Zhou, A. Q. Liu, D. P. Tsai, *Nano Letters* **2014**, *14*, 1 225.

[6] Y. W. Huang, W. T. Chen, W. Y. Tsai, P. C. Wu, C. M. Wang, G. Sun, D. P. Tsai, *Nano Letters* **2015**, *15*, 5 3122.

[7] Z. Huang, D. L. Marks, D. R. Smith, *Optica* **2019**, *6*, 2.

[8] S. Shrestha, A. C. Overvig, M. Lu, A. Stein, N. Yu, *Light: Science & Applications* **2018**, *7* 85.

[9] N. Yu, P. Genevet, M. A. Kats, F. Aieta, J. P. Tetienne, F. Capasso, Z. Gaburro, *Science* **2011**, *334*, 6054 333.

[10] S. Sun, K. Y. Yang, C. M. Wang, T. K. Juan, W. T. Chen, C. Y. Liao, Q. He, S. Xiao, W. T. Kung, G. Y. Guo, L. Zhou, D. P. Tsai, *Nano Letters* **2012**, *12*, 12 6223.

[11] R. Wang, Q. Wu, W. Cai, Q. Zhang, H. Xiong, B. Zhang, J. Qi, J. Yao, J. Xu, *ACS Photonics* **2019**, *6*, 7 1774.

[12] C. Tang, J. Yang, Y. Wang, J. Cheng, X. Li, C. Chang, J. Hu, J. Lü, *Sensors and Actuators B: Chemical* **2021**, *329* 129113.

[13] R. Daniel, T. Andreas, A.-B. Nadine, J.-H. Aurelian, L. Odeta, K. Christopher, Y. Daehan, J. W. Nathan, O. Sang-Hyun, A. L. Hilal, A. Hatice, *Nature Communications* **2018**.

[14] S. Keren-Zur, M. Tal, S. Fleischer, D. M. Mittleman, T. Ellenbogen, *Nature Communications* **2019**, *10*, 1 1778.

[15] E. V. Melik-Gaykazyan, M. R. Shcherbakov, A. S. Shorokhov, I. Staude, I. Brener, D. N. Neshev, Y. S. Kivshar, A. A. Fedyanin, *Philos Trans A Math Phys Eng Sci* **2017**, *375*, 2090.

[16] R. Daniel, T. Andreas, A. B. Nadine, J. H. Aurelian, L. Odeta, K. Christopher, Y. Daehan, N. J. Wittenberg, O. Sang-Hyun, H. A. Lashuel, *Nature Communications* **2018**, *9*, 1 2160.

[17] Tittl, Andreas, Leitis, Aleksandrs, Liu, Mingkai, Yesilkoy, Filiz, Choi, Duk-Yong, *Science* **2018**, *360*, Jun.8 TN.6393 1105.

[18] M. Gupta, R. Singh, *Advanced Optical Materials* **2016**, *4*, 12 2119.

[19] A. E. Miroshnichenko, S. Flach, Y. S. Kivshar, *Reviews of Modern Physics* **2010**, *82*, 3 2257.

[20] W. X. Lim, R. Singh, *Nano Converg* **2018**, *5*, 1 5.

[21] Y. Sonnefraud, N. Verellen, H. Sobhani, G. A. Vandenbosch, V. V. Moshchalkov, P. Van Dorpe, P. Nordlander, S. A. Maier, *ACS Nano* **2010**, *4*, 3 1664.

[22] Z. Chen, S. Zhang, Y. Chen, Y. Liu, P. Li, Z. Wang, X. Zhu, K. Bi, H. Duan, *Nanoscale* **2020**, *12*, 17 9776.

[23] F. Hao, P. Nordlander, Y. Sonnefraud, P. V. Dorpe, S. A. Maier, *ACS Nano* **2009**, *3*, 3 643.

[24] L. Xu, K. Zangeneh Kamali, L. Huang, M. Rahmani, A. Smirnov, R. Camacho-Morales, Y. Ma, G. Zhang, M. Woolley, D. Neshev, A. E. Miroshnichenko, *Advanced Science* **2019**, *6*, 15 1802119.

[25] N. Liu, M. Hentschel, T. Weiss, A. P. Alivisatos, H. Giessen, *Science* **2011**, *332*, 6036 1407.

[26] M. Hentschel, M. Saliba, R. Vogelgesang, H. Giessen, A. P. Alivisatos, N. Liu, *Nano Letters* **2010**, *10*, 7 2721.

[27] Kirill, Koshelev, Sergey, Lepeshov, Mingkai, Liu, Andrey, Bogdanov, Yuri, Kivshar, *Physical Review Letters* **2018**, *121*, 19 193903.

[28] C. W. Hsu, B. Zhen, A. D. Stone, J. D. Joannopoulos, M. Soljačić, *Nature Reviews Materials* **2016**, *1*, 9 16048.

[29] M. Liu, D.-Y. Choi, *Nano Letters* **2018**, *18*, 12 8062.

[30] L. Xu, M. Rahmani, Y. Ma, D. A. Smirnova, K. Z. Kamali, F. Deng, Y. K. Chiang, L. Huang, H. Zhang, S. Gould, D. N. Neshev, A. E. Miroshnichenko, *Advanced Photonics* **2020**, *2*, 02 1.

[31] D. R. Abujetas, N. van Hoof, S. ter Huurne, J. G. Rivas, J. A. Sánchez-Gil, *arXiv:1901.03122* **2019**.

[32] Y. K. Srivastava, R. T. Ako, M. Gupta, M. Bhaskaran, S. Sriram, R. Singh, *Applied Physics Letters* **2019**, *115*, 15 151105.

[33] X. Chen, W. Fan, H. Yan, *Optics Express* **2020**, *28*, 11 17102.

[34] V. Savinov, V. A. Fedotov, N. I. Zheludev, *Physical Review B* **2014**, *89*, 20.

[35] Y. He, G. Guo, T. Feng, Y. Xu, A. E. Miroshnichenko, *Physical Review B* **2018**, *98*, 16.

[36] X. Liu, Z. Liu, M. Hua, L. Wang, K. Wang, W. Zhang, Y. Ning, Y. Shi, X. Wang, F. Yang, *ACS Applied Nano Materials* **2020**, *3*, 3 2129.

[37] A. Cerjan, M. Jurgensen, W. A. Benalcazar, S. Mukherjee, M. C. Rechtsman, *Physical Review Letters* **2020**, *125*, 21 213901.

[38] J. Jin, X. Yin, L. Ni, M. Soljacic, B. Zhen, C. Peng, *Nature* **2019**, *574*, 7779 501.

[39] D. R. Abujetas, A. Barreda, F. Moreno, A. Litman, J. Geffrin, J. A. SánchezGil, *Laser & Photonics Reviews* **2020**, *15*, 1.

[40] B. Ferguson, X. Zhang, *Nature Materials* **2002**, *1* 26.

[41] D. Suzuki, S. Oda, Y. Kawano, *Nature Photonics* **2016**, *10* 809.

[42] G. Liu, C. Chang, Z. Qiao, K. Wu, Z. Zhu, G. Cui, W. Peng, Y. Tang, J. Li, C. Fan, *Advanced Functional Materials* **2019**, *29*, 7 1807862.

[43] W. Shi, Y. Wang, L. Hou, C. Ma, L. Yang, C. Dong, Z. Wang, H. Wang, J. Guo, S. Xu, *Journal of Biophotonics* **2021**, *14*, 1 e202000237.

[44] T. C. W. Tan, E. Plum, R. Singh, *Advanced Optical Materials* **2020**, *8*, 6 1901572.

[45] P. Zarogoulidis, L. Yarmus, K. Zarogoulidis, *Therapeutic delivery* **2013**, *4*, 10 1221.

[46] N. Kumari, B. S. Dwarakanath, A. Das, A. N. Bhatt, *Tumor Biology* **2016**, *37*, 9 11553.

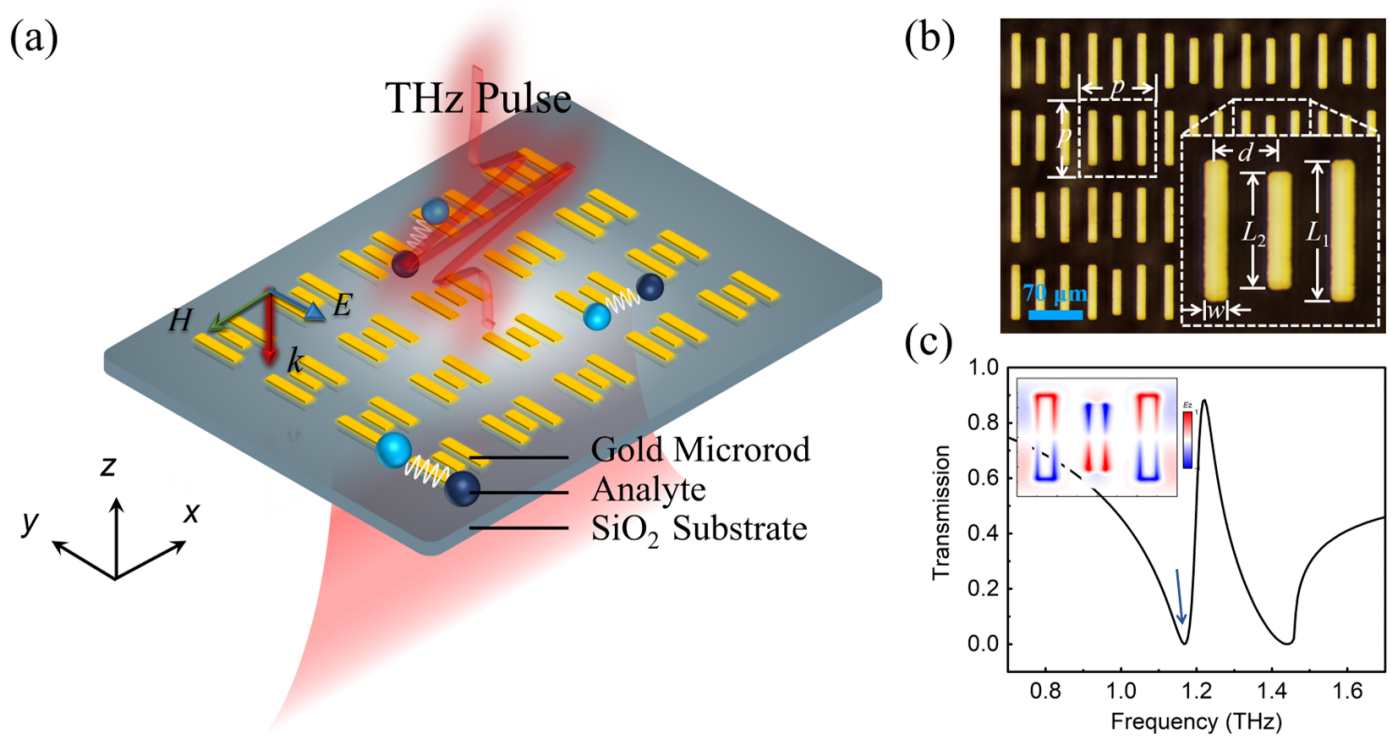

Figure 1: a) Schematic view of the proposed metasurface structure supporting Fano resonance quasi-BIC. b) Optical image of the metasurface. The inset depicts the geometrical parameters of the unit cell composed of three gold rods, with a periodicity p of 100 μm. The space between the rods is $d = 32$ μm. Width $w = 10$ μm, one of the rods has a fixed dimension of $L_1 = 70$ μm, whereas the other L_2 varies as shown at the center. c) Calculated transmission spectrum of the metasurface with structural parameter $L_2 = 55$ μm. The inset shows the electrical distribution of E_z at the resonance frequency $f = 1.17$ THz.

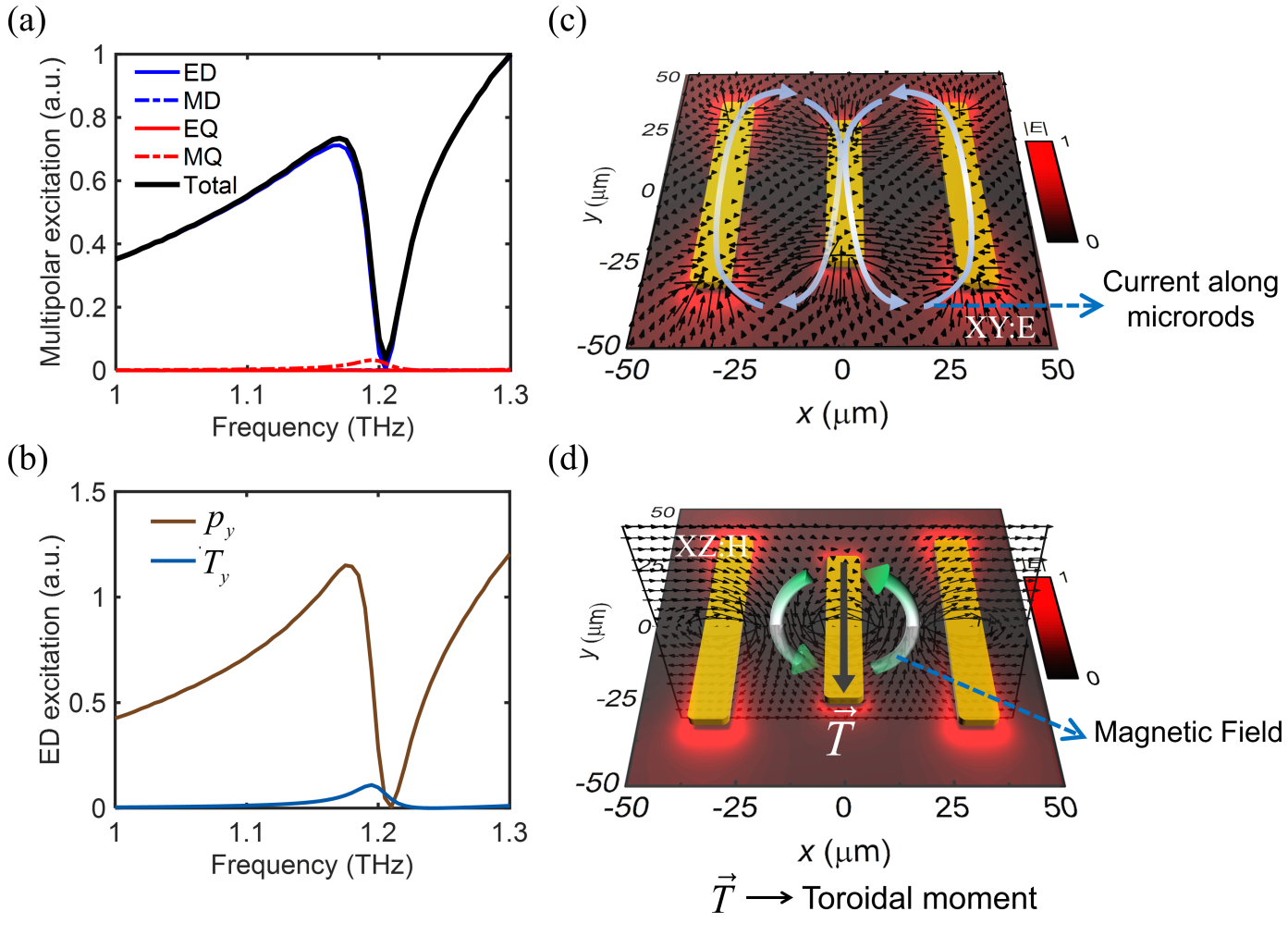

Figure 2: a) Spherical multipolar structure of the metasurface. b) Cartesian ED and TD excitations of the metasurfaces. c) Calculated electric near-field distributions with induced surface current along microrods at the resonant spectral position $f = 1.17$ THz at XY plane(XY: E). The arrows indicate the electric field directions. d) Torodial configutation with magnetic field. The arrows stand for the magnetic field vectors at the XZ plane (XZ: H).

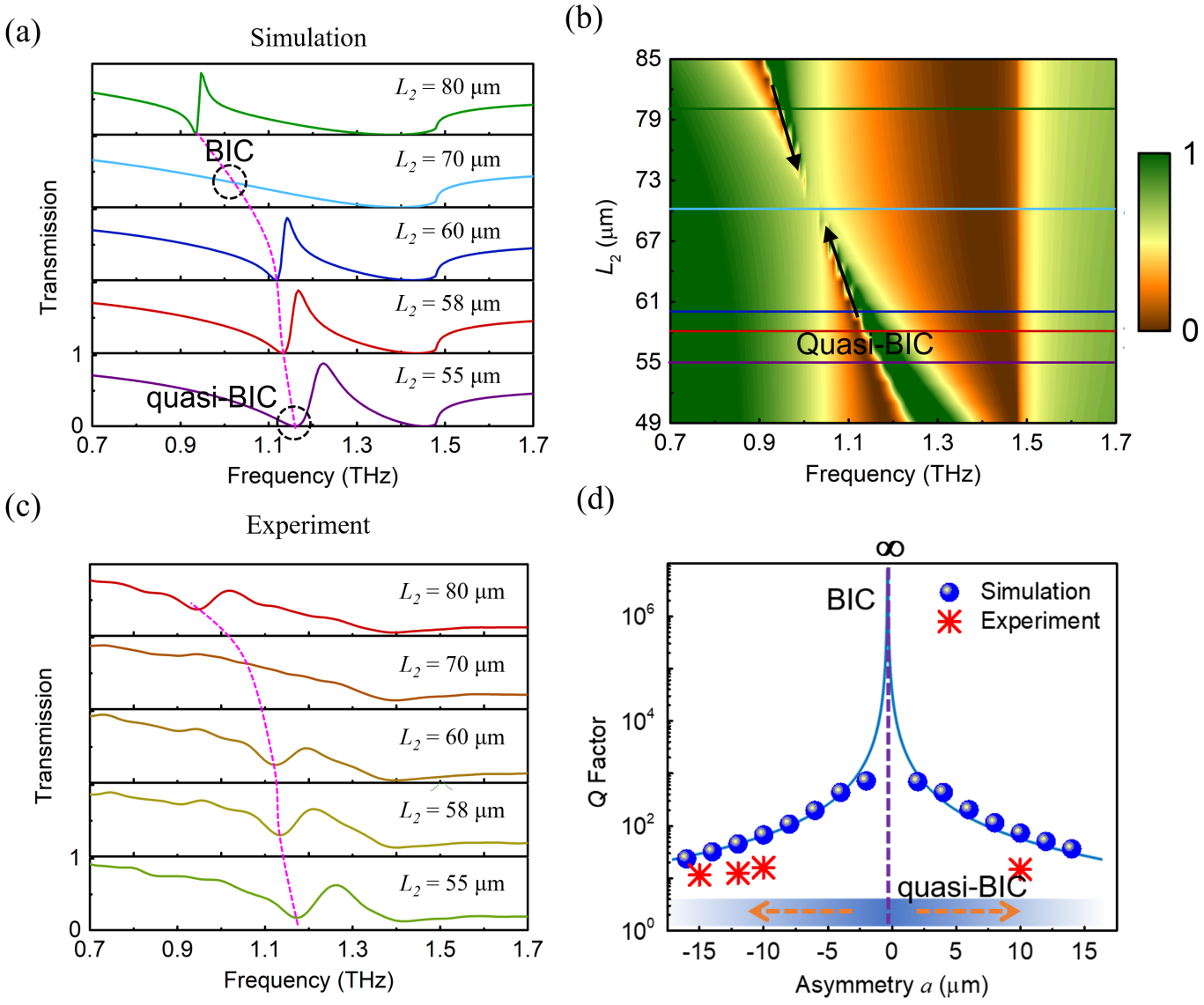

Figure 3: a,b) Simulated transmission spectra of the proposed structure with different parameter L_2. c) Experimental transmission spectral evolution is in good agreement with the simulation. The dash lines trace the evolution of the transmission dips. d) Q factor of the simulated (sphere) and experimental (star) quasi-BIC Fano resonance as a function of asymmetry a.

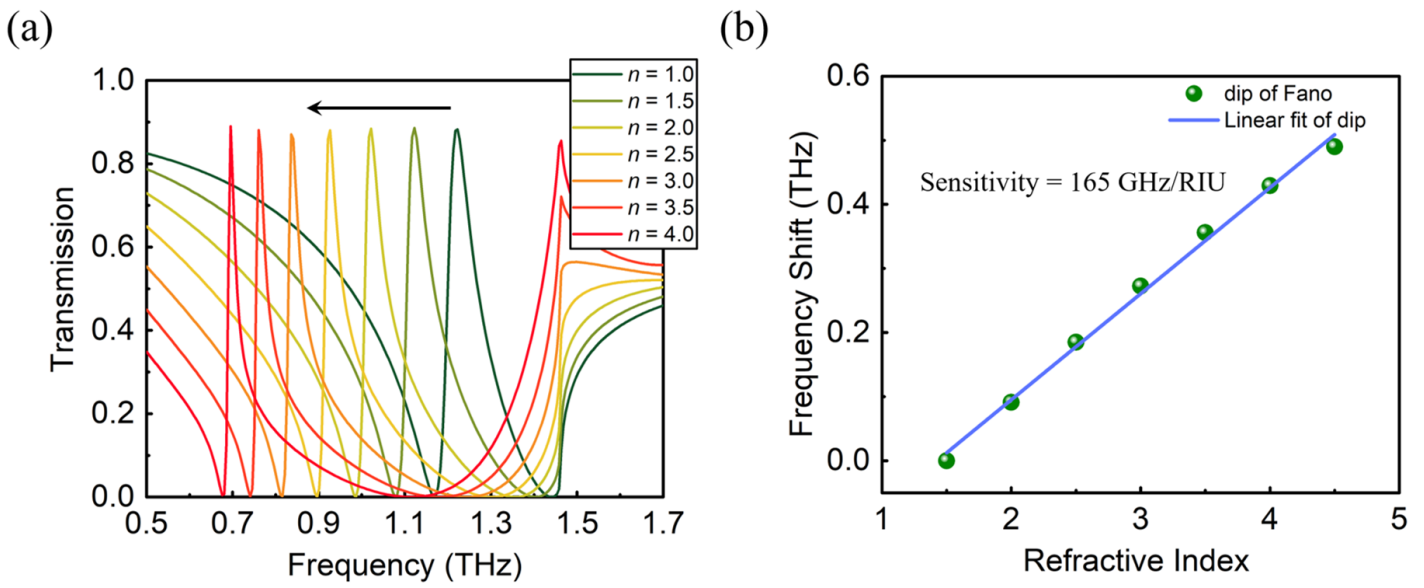

Figure 4: a) Transmission spectra of different refractive index of analyte varied from 1 to 4 with fixed thickness of 6 μm. b) Frequency shift of dip with different refractive indices of the analyte.

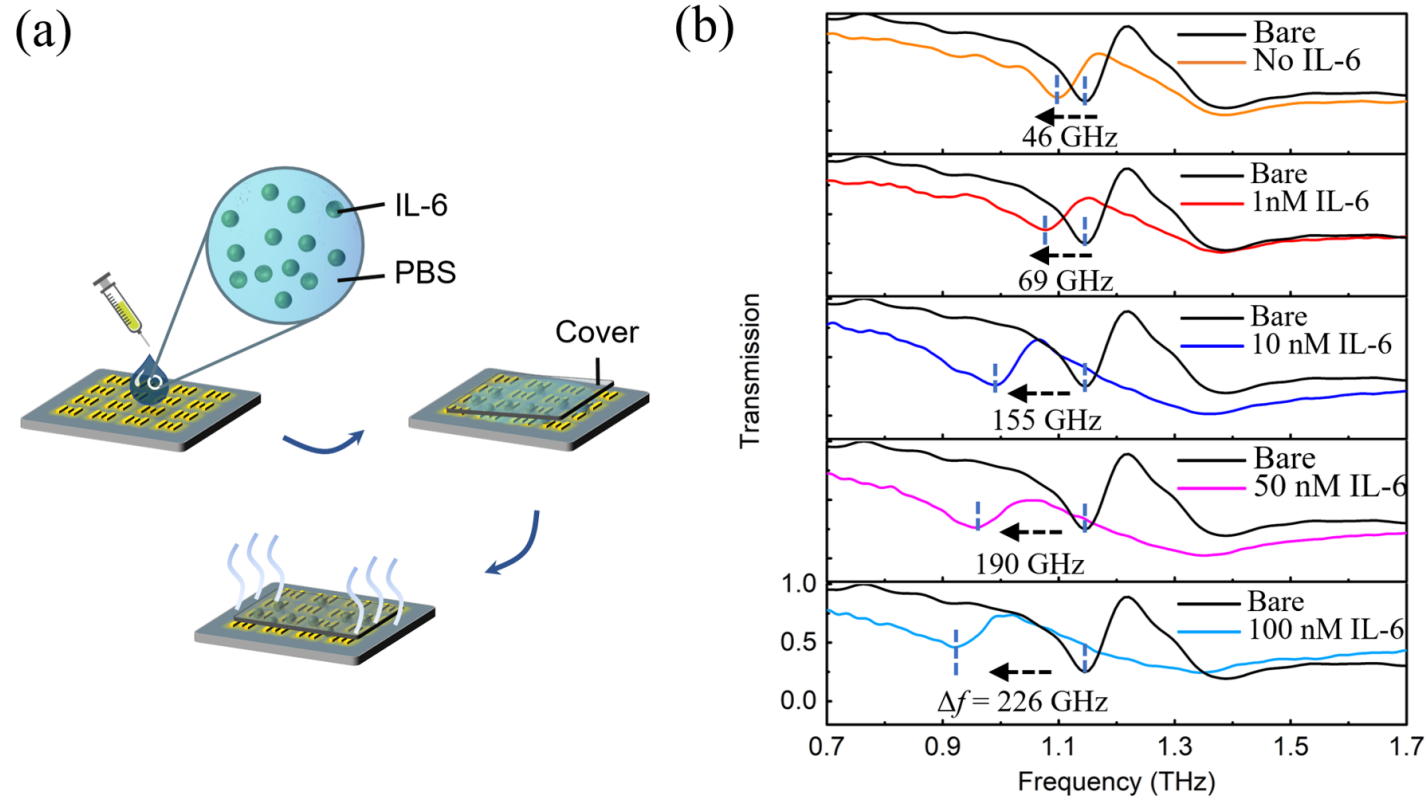

Figure 5: a) Flow process diagram of sample preparation. b) Measured transmission spectra of the designed metasurface-based biosensors with different IL-6 concentrations: bare (No IL-6/PBS), 0 nM (No IL-6 in PBS), 1 nM, 10 nM, 50 nM, and 100 nM.